Materials Today Communications 32 (2022) 103995

Contents lists available at ScienceDirect

Materials Today Communications

journal homepage: www.elsevier.com/locate/mtcomm

Ground-state properties of p-type delafossite transparent conducting oxides 2H-$CuMO_2$ (M=Al, Sc and Y): DFT calculations

Moufdi Hadjab [a,b,*], Olga Guskova [b,c], Hamza Bennacer [a], Mohamed Issam Ziane [d], Abderrahim Hadj Larbi [e], M.A. Saeed [f]

[a] Electronics Department, Faculty of Technology, Mohamed Boudiaf University of M'sila, M'sila 28000, Algeria
[b] Leibniz Institute of Polymer Research Dresden Institute of Theory of Polymers, 01069 Dresden, Germany
[c] Technische Universität Dresden, Dresden Center for Computational Materials Science (DCMS), 01062 Dresden, Germany
[d] École Supérieur en Génie Électrique et Énergétique d'Oran (ESGEE), Oran 31000, Algeria
[e] Research Center in Industrial Technologies CRTI, P.O. Box 64, Cheraga 16014, Algiers, Algeria
[f] Department of Physics, Division of Science & Technology, University of Education, Lahore, Pakistan

ARTICLE INFO

Keywords:
First-principles calculations
FP-LAPW
Delafossite transparent conducting oxides
$CuMO_2$
Optoelectronic properties
Structural parameters

ABSTRACT

In this study, we have investigated physical ground-state properties of three novel semiconductors to address many problems related to the photovoltaic (PV) industry. A computational package (wien2k) based on Density Functional Theory (DFT) is used to study the optical, structural, as well as electronic properties of delafossite transparent conducting oxides $CuMO_2$ (M= Al, Sc and Y). The Full-Potential Linearized Augmented Plan Wave method (FP-LAPW) which is based on DFT has also been employed in this study. To compute the structural and electronic parameters the Local Density Approximation (LDA), Perdew, Burke and Ernzerhof Generalized Gradient Approximation (PBE-GGA) have been utilized as the exchange-correlation term. Furthermore, Tran-Blaha modified Beck–Johnson potential (TB-mBJ) has been utilized to achieve better degree of accuracy in computing the electronic and optical characteristics. The results of the study have also been compared to the previous theoretical and experimental ones. The ternary delafossite transparent conducting oxide compounds can be considered as an alternative material in photovoltaic applications.

1. Introduction

Due to the high optical transparency (~80–90%) and electrical conductivity (~10^4 S cm^{-1}), transparent conducting oxides (TCOs) are widely used in optoelectronic applications and therefore, have been studied extensively [1–6]. The scope of TCOs is increasing due to their higher performance in many applications like low-emissive window layers, transparent contacts of flexible photovoltaic solar cells including large-area displays, touch screens, gas sensors, electromagnetic shielding, biosensors, light emitting diodes and other optoelectronic devices based on organic/inorganic and biological materials at the macro/meso/nano-scale [7–11].

The TCOs are primarily studied as binary compounds like; In_2O_3, SnO_2, ZnO, CdO etc. [3,7], however some TCOs such as Zn_2SnO_4, $ZnSnO_3$, $MgIn_2O_4$, $GaInO_3$, $(Ga,In)_2O_3$, $Zn_2In_2O_5$, $In_4Sn_3O_{12}$, $LiGaCr_4O_8$, $LiInCr_4O_8$, $GdCrO_3$, $(C_6H_{10}N_2)_2[Co(H_2O)_4P_2Mo_5O_{23}]$, $La_{0.75}Sr_{0.25}MnO_3$, $LaRO_3$, $Ba_{1-x}Sr_xFeO_3$, $BaSnO_3$ [7,12–19] have also been reported.

Literature suggested that, there are only few reports available regarding fabrication of active devices with TCOs [7]. The use of TCOs as transparent electrodes has been well-established due to the n-type nature of these semiconductors [5]. These types of semiconductors exhibit high hole effective mass caused by the localized Oxygen-2*p* (O-2*p*) orbitals, which is the key contributor of valence band maximum (VBM) [3,20].

Consequently, many scientific efforts have been reported during the last decade of 20^{th} century regarding search for new and efficient p-type TCOs [7,20,21]. The major emphasis was on reducing the hole effective mass by delocalizing the O-2*p* orbitals via strong hybridization with electronic orbitals of the third atom [3,7]. Hosono et al. [13] proposed an idea demonstrating the strong hybridization between metallic *d* orbitals and O-2*p* orbitals resulted as an increment in VBM level that would ultimately eases the doping [20]. The discovery of new Cu^+-based p-type TCOs such as $CuAlO_2$, $CuScO_2$ and $CuYO_2$ revealed that closed shell configuration of Cu^+ favours the hybridization of Cu-3*d* energy

* Corresponding author at: Electronics Department, Faculty of Technology, Mohamed Boudiaf University of M'sila, M'sila 28000, Algeria.
E-mail address: moufdi.hadjab@univ-msila.dz (M. Hadjab).

https://doi.org/10.1016/j.mtcomm.2022.103995
Received 27 April 2022; Received in revised form 2 July 2022; Accepted 10 July 2022
Available online 14 July 2022

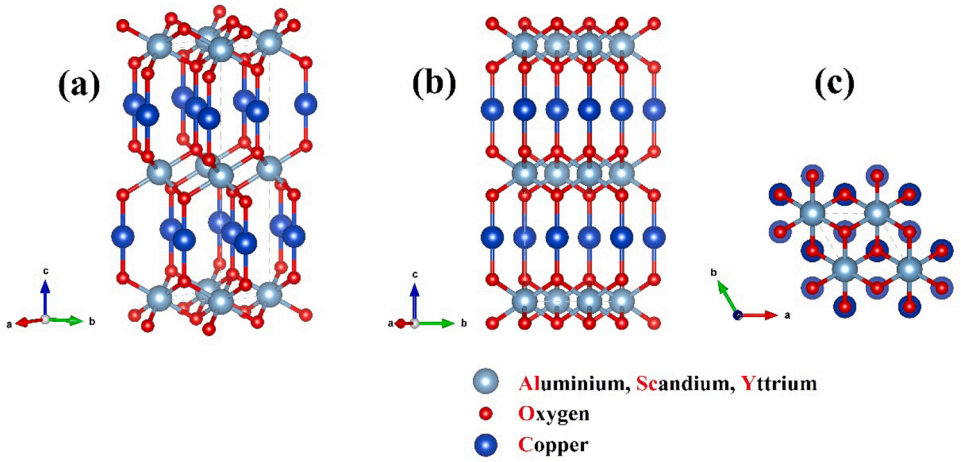

Fig. 1. Crystal structure of $CuMO_2$ (M= Al, Sc and Y) delafossite with hexagonal bases, (a, b) 3D section and c) 2D top section.

level with the O-2*p* level in addition to the wide band gap and optical transparency of these materials [20,21].

Delafossite materials with chemical formula $A^{I}B^{III}O_2$ are among the promising p-type TCOs [3,22]. $CuAlO_2$ was one of the very first delafossite transparent oxides that demonstrated p-type conductivity and high optical transparency [21]. This compound is very important for the p-n junction of TCO and can help to fabricate highly efficient thin film solar cells [23], because it has a wider band gap (> 3 eV) as compared to the binary TCOs with a strong hybridization between A-*d* and O-2*p* orbitals [3].

$CuAlO_2$ is one of the most investigated Cu-based delafossites. According to Bhamu et al., It crystallizes in either 3R-rhombohedral or 2H-hexagonal structure with space group # 166 and 194, respectively [24]. This type of compound is dedicated for absorbing the radiations in solar cells, photo-electrochemical devices or photovoltaics [24,25]. At the same time, this material has been widely studied both theoretically [5, 23–31] and experimental [7,8,27,32–36] to explore high-performance and low-cost TCOs [36]. To the best of the authors' knowledge, there are still no in-depth descriptions of the linear optical properties of $CuYO_2$ and $CuScO_2$. Therefore, it is indispensable to investigate systematically the relevant structural, electronic and optical properties of p-type delafossite oxides.

2. Computational details

The optoelectronic and structural properties of p-type delafossite transparent conducting oxides 2H-$CuMO_2$ (M=Al, Sc and Y) (see Fig. 1) are investigated using Full Potential Linearized Augmented Plane Wave (FP-LAPW) method via Wien2k Tool within the framework of DFT [37–39].

The FP-LAPW method has emerged as an extensively used very robust and accurate state-of-the-art first-principles electronic structure technique with reasonable computational efficiency to simulate the physical properties of solid-state materials based on DFT [40]. In this technique, the unit cell is divided into non-overlapping muffin-tin (MT) spheres around the atomic locations and the interstitial area using different basis sets for these areas [41].

The Local Density Approximation (LDA) [42,43] and the revised Perdew-Burke-Ernzerhof Generalized Gradient Approximation (PBE-sol-GGA) [44] have been utilized as the exchange–correlation terms to investigate the structural and electronic parameters. Moreover, for better degree of accuracy in calculations, Tran-Blaha modified Beck–Johnson potential (TB-mBJ) [45] was also used. The TB-mBJ method is used to calculate the imaginary as well as real parts of the dielectric function. The same method is also employed to investigate the reflectivity, refractive index, optical conductivity, absorption coefficient and the energy loss function to understand the linear optical properties of delafossite TCOs i.e., $CuAlO_2$, $CuScO_2$ and $CuYO_2$. This approach/-method proposed by Tran and Blaha leads to a better description of semiconductors and insulators compared to the standard approximations. The TB-mBJ potential can be written as:

$$\upsilon_{x,\sigma}^{mBJ}(r) = c\upsilon_{x,\sigma}^{BR}(r) + (3c-2)\frac{1}{\pi}\sqrt{\frac{5}{12}\sqrt{\frac{2\tau_\sigma(r)}{\rho_\sigma(r)}}} \quad (1)$$

where ρ_σ is the electron density, τ_σ is the kinetic-energy and $\upsilon_{x,\sigma}^{BR}$ is the Becke-Roussel potential [46]. Herein, a system-dependent parameter *c* represents the Becke-Johnson potential $c= 1$ as an original value. However, for the bulk materials, this parameter can be calculated as proposed by Tran and Blaha [41]:

$$c = \alpha + \beta\left(\frac{1}{V_{cell}}\int\frac{|\nabla\rho_\sigma(r')|}{\rho_\sigma(r')}d^3r'\right)^{\frac{1}{2}} \quad (2)$$

where V_{cell} represents the volume of unit cell, α (−0.012) and β (1.023) $bohr^{1/2}$ are fitting parameters as per experimental data [45]. For electronic structures calculations of materials, the TB-mBJ is one of the important exchange potentials that can produce significantly improved band gaps [41].

The TB-mBJ improves the energy gap by modifying the potential Vxc, but how physically this happens? I mean between electrons and orbitals.

It is well-documented that adding the Hartree-Fock (HF) exchange to the energy functional can alter significantly the energy band gap of solids with two extremists: pure HF which overestimates energy band gap and a local density approximation LDA (or generalized gradient approximation GGA functional) of DFT which underestimates the energy band gap. This is the main reason behind the good performance of hybrid XC in computing the energy band gap where a portion of HF exchange is used.

The plane wave expansion was taken as $R_{MT}\times K_{MAX} = 8$, where RMT represents the smallest Muffin-Tin radius and K_{MAX} represents the highest K-vector of Brillouin Zone (BZ). The Muffin-Tin Radii (RMT) were taken as 1.74, 1.69, 1.62, 2.15 and 1.55 a.u. for Cu, Al, Sc, Y and O, respectively, for the delafossite transparent conducting oxides. The cut-off for the Fourier-expanded charge density was set at $G_{max}= 14$ $(a.u.)^{-1}$. The expansion in spherical harmonic functions inside the non-overlapping MT spheres is expanded up to $l_{max}= 10$. The cut-off energy is set to be − 6 Ryd for the separating core states from valence states. For the irreducible wedge, there are 1000 k-points in the BZ, (60, 54 and 81 special k-points in the reduced wedge) for the calculations of

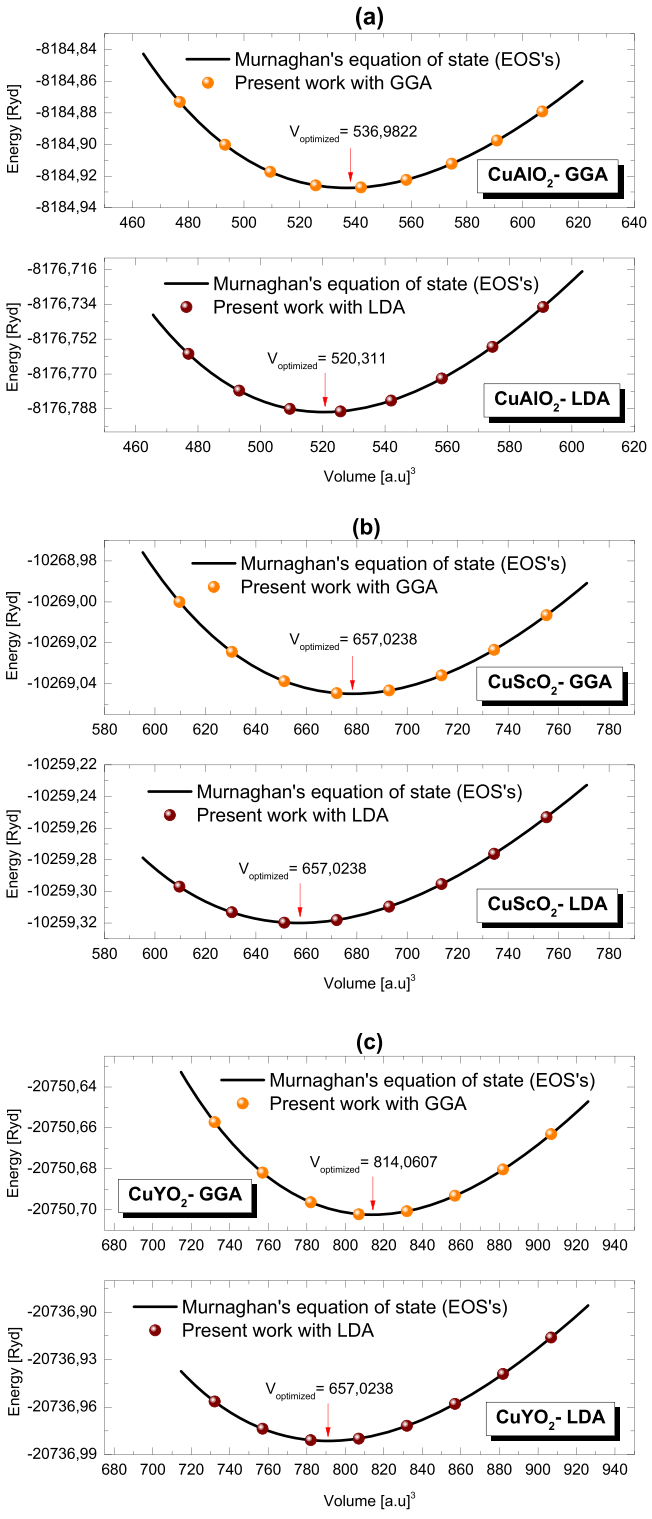

Fig. 2. Calculated total energy as a function of unit cell volume for a) $CuAlO_2$, b) $CuScO_2$ and c) $CuYO_2$ within LDA and PBEsol-GGA.

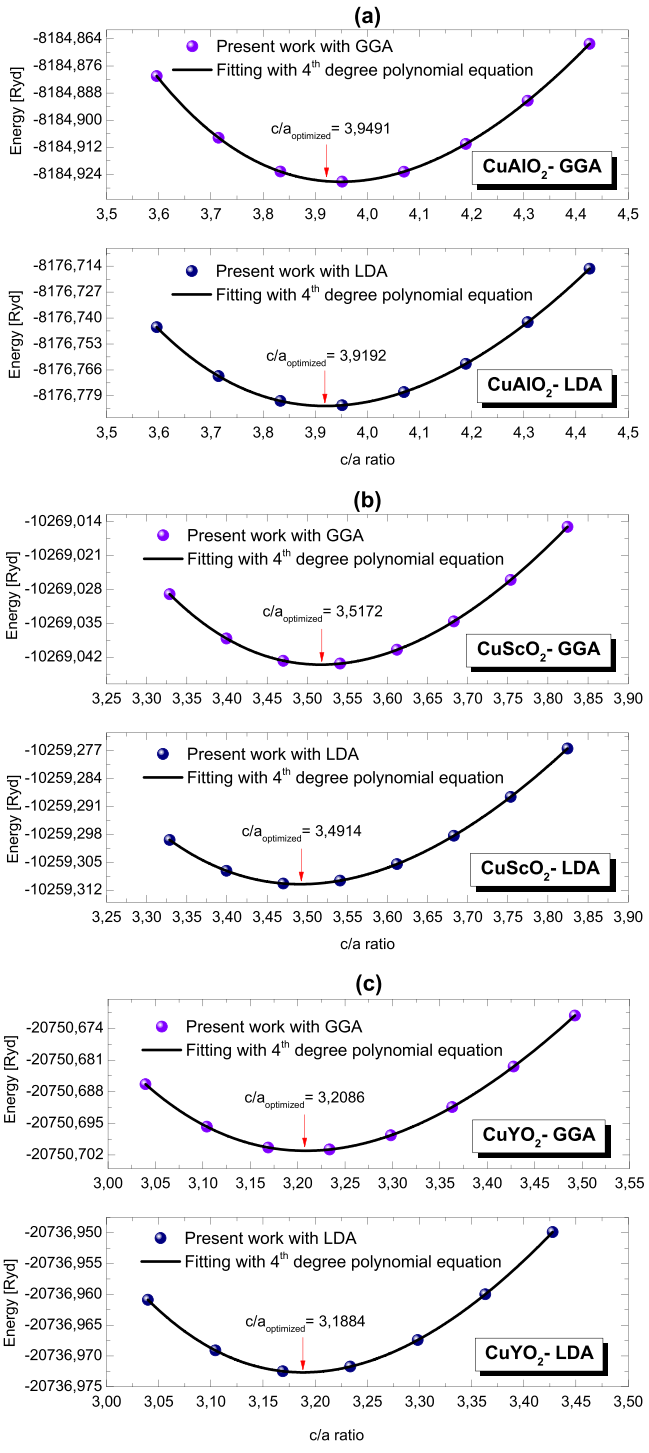

Fig. 3. Calculated total energy as a function of c/a ratio for a) $CuAlO_2$, b) $CuScO_2$ and c) $CuYO_2$ within LDA and PBEsol-GGA.

structural and electronic properties for $CuAlO_2$, $CuScO_2$ and $CuYO_2$ respectively. In the linear optical calculations section, we utilized a fine *k*-mesh of 2500 k-points for the reason that the prediction of linear optical properties necessitates a dense mesh of eigenvalues and the corresponding eigenvectors.

The **Cu**: 1 s^2 $2s^2$ $2p^6$ $3s^2$ $3p^6$ $3d^{10}$ $4s1$, **Al**: $1s^2$ $2s^2$ $2p^6$ $3s^2$ $3p^1$, **Sc**: $1s^2$ $2s^2$ $2p^6$ $3s^2$ $3p^6$ $3d^1$ $4s^2$, **Y**: $1s^2$ $2s^2$ $2p^6$ $3s^2$ $3p^6$ $3d^{10}$ $4s^2$ $4p^6$ $4d^1$ $5s^2$, **O**: $1s^2$ $2s^2$ $2p^4$ electrons are explicitly treated as valence electrons.

3. Results and discussions

The lattice constants (*a*, *c*), bulk modulus (*B*), band-gap energies (Eg), density of states (DOS) and the linear optical properties represented by the refractive index $n(\omega)$, dielectric function $\varepsilon(\omega)$, absorption coefficient $a(\omega)$, optical conductivity $\kappa(\omega)$, reflectivity $R(\omega)$ and the electron energy loss $L(\omega)$ for the three delafossites-oxides have been investigated to access their applications.

Table 1
Calculated lattice constants (a and c), internal parameter (z_O), bulk modulus (B) and its first pressure derivative (B') according to LDA and PBEsol-GGA approximations for the p-type delafossite transparent conducting oxides 2H-$CuMO_2$ (M=Al, Sc and Y), compared with other experimental and theoretical previous works.

	$a = b$ (Å)	c/a	c (Å)	z_O (Å)	B (GPa)	B'
2H-$CuAlO_2$						
Our results (LDA)	**2.832**	**3.92**	**11.10**	**0.0855**	**209.401**	**4.385**
Our results (PBEsol-GGA)	**2.854**	**3.95**	**11.274**	**0.0855**	**192.194**	**4.294**
Experimental results	2.863 [48]	3.951 [48]	11.314 [48]	0.0851 [48]	–	–
	2.858 [52]	3.951 [52]	11.293 [52]	0.0859 [52]		
Other theoretical calculations	2.856 [25]	4.014 [25]	11.466 [25]	0.0835 [25]	211 [25]	–
	2.797 [26]	3.977 [26]	11.125 [26]	-	-	
	2.849 [50]	3.985 [50]	11.355 [50]	0.0855 [51]	-	
	2.798 [51]	3.98 [51]	11.135 [51]	0.0843 [51]		
	2.819 [51]	3.998 [51]	11.272 [51]			
2H-$CuScO_2$						
Our results (LDA)	**3.181**	**3.491**	**11.107**	**0.0897**	**172.46**	**4.592**
Our results (PBEsol-GGA)	**3.207**	**3.517**	**11.281**	**0.0894**	**156.313**	**4.42**
Experimental results	3.223 [48]	3.541 [48]	11.413 [48]	0.0893 [48]	–	–
Other theoretical calculations	3.308 [50]	3.437 [50]	11.372 [50]	- 0.090 [51]	–	–
	3.172 [51]	3.528 [51]	11.192 [51]	0.0894		
	3.236 [51]	3.512 [51]	11.367 [51]			
2H-$CuYO_2$						
Our results (LDA)	**3.488**	**3.188**	**11.122**	**0.0908**	**145.067**	**4.63**
Our results (PBEsol-GGA)	**3.514**	**3.208**	**11.277**	**0.0904**	**132.446**	**4.45**
Experimental results	3.531 [25]	3.233 [25]	11.418 [25]	0.0893 [25]	–	–
	3.522 [49]	3.242 [49]	11.42 [49]	- 0.0893		
	3.52 [53]	3.242 [53]	11.418 [43]			
Other theoretical calculations	3.54 [25]	3.282 [25]	11.62 [25]	0.0894 [25]	126 [25]	–
	3.628 [50]	3.142 [50]	11.402 [50]	- 0.091 [51]	-	
	3.476 [51]	3.221 [51]	11.197 [51]			

3.1. Structural properties

The 2H-$CuMO_2$ (M=Al, Sc and Y), p-type delafossite TCOs are crystallizes in hexagonal structure ($P6_3/mmc$, no. 194) with Cu atom located at (1/3, 2/3, 1/4) while Al, Sc and Y are sited at (0, 0, 0) and O at (1/3, 2/3, z_O) position.

The experimental lattice constants 'a' and 'c' are utilized as input parameters in the current study to optimize the structural properties. The optimization was performed by the following four steps as mentioned below:

- To obtain the value of the internal cell parameter z_O, the constituent atoms needs to be at energetically favourable positions and for this atom are relaxed by reducing/minimizing the initial crystal structures.
- The energy-volume curve needs to be fitted with the Murnaghan's Equation of State (EOS) [47] to obtain various structural parameters such as lattice parameter a, and bulk modulus B as well as its first pressure derivative B'.
- To find out c/a ratio, the total energy needs to be fitted via 4th degree polynomial equation for each material.
- And for the final optimization of structural parameters of the delafossite oxides 2H-$CuMO_2$, we have to exploit the volume expression, where; M= Al, Sc and Y.

For the three oxides using LDA and PBEsol-GGA approximations, the total energy versus unit cell volume and the c/a ratio respectively is shown in Figs. 2 and 3 whereas the optimized structural properties are given in Table 1. The theoretically computed results are in good agreement with the previous results *i.e.* Experimental [48,49,52,53] as well as theoretical ones [25,26,50,51]. The electronic and linear optical properties will be investigated by utilizing the optimized volume and c/a ratio.

3.2. Electronic properties

The potential understanding of the semiconducting gap comes from the symmetry and position of atoms, which thus agree the occupation of band energy levels around the Fermi level (EF) [54].

The viability of the delafossite transparent conducting oxides $CuMO_2$ (M= Al, Sc and Y) in optoelectronic applications necessitate bit in-depth investigation of their electronic properties like energy band structure, band-gap values and Total/Partial density of states (TDOS/PDOS). The band-gap values of the three delafossite oxides with hexagonal phase have been predicted using LDA, PBEsol-GGA and TB-mBJ approaches and are listed in Table 2. The results obtained for TB-mBJ are given here, similar patterns were observed for other approximations. The band structures in energy range from − 10–21 eV were evaluated via TB- mBJ approximation along the high symmetry directions; Γ → M → K → Γ → A → L → H → A in the BZ. The bottom of conduction band and top of the valence band are at different k-value demonstrating the indirect band-gap nature of the delafossite crystals when the EF is set at 0 eV. For all three considered delafossite oxides 2H-$CuMO_2$ (Al, Sc and Y), predicted band structures and their corresponding projected density of states (TDOS) for each in equivalent atom are displayed in Fig. 4(a, b and c)

Table 2
Calculated indirect band-gaps (Eg) according to LDA, GGA-PBEsol and the mBJ approximations for the p-type delafossite transparent conducting oxides 2H-$CuMO_2$ (M=Al, Sc and Y), compared with other experimental and theoretical previous works.

Materials	Indirect energy band-gaps values [eV]				
	LDA	PBEsol-GGA	mBJ	Exp.	Others (theoretical)
2H-$CuAlO_2$	**2.227**	**1.962**	**2.279**	1.8 [57]	2.23 [24], 2.2 [24,26], 1.82 [55], 1.9 [56], 2.194 [31], 1.878 [31], 1.905 [31]
2H-$CuScO_2$	**2.391**	**2.37**	**2.388**	3.7 [5][a]	2.25 [50], 2.27 [50]
2H-$CuYO_2$	**2.664**	**2.694**	**2.838**	3.5 [5][a]	2.62 [50], 2.67 [50]

[a] These values are obtained in 3R-rhombohedral structure with space group R-3 m (No. 166)

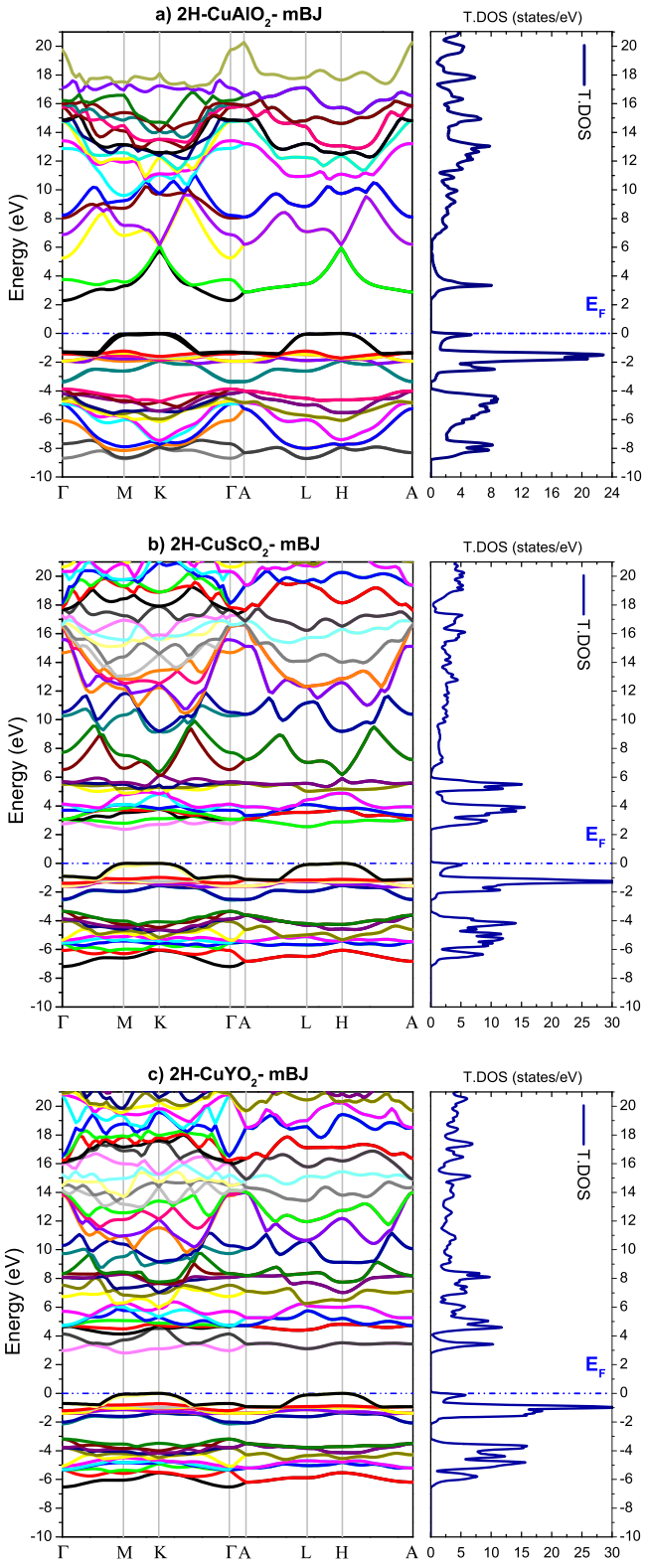

Fig. 4. Band structure and TDOS for a) $CuAlO_2$, b) $CuScO_2$ and c) $CuYO_2$ within mBJ approximation.

demonstrating the indirect band-gap nature of all compounds.

The obtained results of calculated indirect band-gaps are listed in Table 1, these calculations are performed according to LDA, PBEsol-GGA and the TB-mBJ approximations for the p-type delafossite transparent conducting oxides 2H-$CuMO_2$ (M=Al, Sc and Y). The observed values of

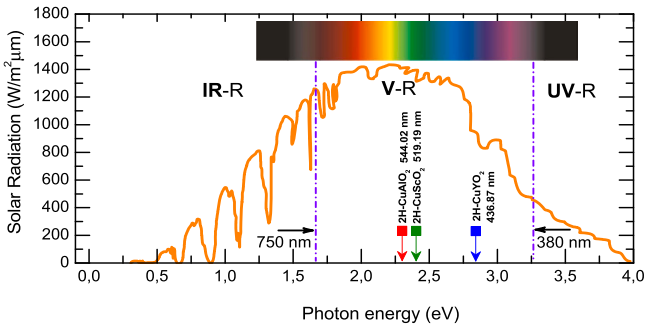

Fig. 5. The spectrum of sun's solar radiation versus energy band gap variation with mBJ of $CuMO_2$ (X=Al, Sc, and Y).

band-gap for each compound are in close agreement with already reported theoretical and experimental calculations.

The evolution of energy band gap calculated by TB-mBJ with the solar spectrum AM 1.5 is shown in Fig. 5. The solar irradiance spectrum comprises of three areas *i.e.* visible region, infrared region (IR), and the ultraviolet (UV) region. The visible region ranges from 380 to 750 nm and IR is for the higher wavelengths and the UV region is for the lower wavelengths. The results reveal a variation in the band gap of three delafossite oxides. This variation indicates a strong absorption in the visible region. This means that the studied materials could be used for the visible optoelectronics applications. In addition, we indicate that, the gap value of $CuYO_2$ is 0.45 eV higher than that of $CuScO_2$ and 0.56 eV higher than that of $CuAlO_2$. The coupling between d orbitals of group-III and O_2*p* states can improve the VBMs, so $CuScO_2$ and $CuYO_2$ have larger VBMs as compared to $CuAlO_2$, which has no *d* electrons. Furthermore, the energy level of Sc_3*d* is inferior to that of Y_4*d*, thus the VBM of $CuScO_2$ is higher among all three delafossite oxides [29]. In context of the atomic configuration, this trend is proportionate with the order of VBMs of $CuAlO_2$, $CuGaO_2$, and $CuInO_2$ [58].

For better understanding the relationship between the different atomic orbital contributions and the electronic band structures [59], the calculated TDOS and PDOS are plotted. Fig. 6 presents the projected densities of states (DOS) for each atom named in the partial density of states (PDOS) along with the Cu_*s/p/d*, Al_*s/p*, Sc_*s/p/d*, Y_*s/p/d* and O_*s/p* for a) $CuAlO_2$, b) $CuScO_2$ and c) $CuYO_2$ using only the TB-mBJ method. The EF in all DOS plots localize at zero eV. The region of energy that is directly above the EF and does not contain any electronic states is the band gap. From the Fig. 6, we found remarkable similarities and unique behaviour between the 2H-$CuAlO_2$, 2H-$CuScO_2$ and 2H-$CuYO_2$ materials. It is obvious that, the DOS are divided into three major areas i.e., low-energy band (VB_{low}), a higher-energy band (VB_{higher}) and a conduction band (CB). The VB_{low} mainly dominated by the O_2*p* orbitals is located in the energy range from − 8.88 to − 3.74 eV for 2 H-$CuAlO_2$, from − 7.26 to − 3.27 eV for 2H-$CuScO_2$ and from − 6.58 to − 3.01 eV for 2 H-$CuYO_2$. The VB_{higher} is situated between − 3.45, − 2.6 and − 2.23 eV for 2 H-$CuAlO_2$, 2H-$CuScO_2$ and 2H-$CuYO_2$, respectively due to Cu_3*d* orbitals. However, the CB is observed from 2.21, 2.26 and 2.76–14 eV for 2 H-$CuAlO_2$, 2H-$CuScO_2$ and 2H-$CuYO_2$, respectively. In addition, the CB of 2H-$CuAlO_2$ is principally composed of a mixture of Cu_3*d* and O_2*p*. For the case of 2H-$CuScO_2$ and 2H-$CuYO_2$, the observed CB is dominated by Sc_3*d* and Y_3*d*, respectively. For 2H-$CuAlO_2$, the main contribution in the TDOS came from Cu and O atoms. However, the observation of CB in 2H-$CuScO_2$ shows that the contribution of the Sc atom in TDOS is prominent, while in the case of 2H-$CuYO_2$ the main contribution in the CB is set by the Y atom.

3.3. Optical properties

The linear optical properties of proposed oxides like dielectric

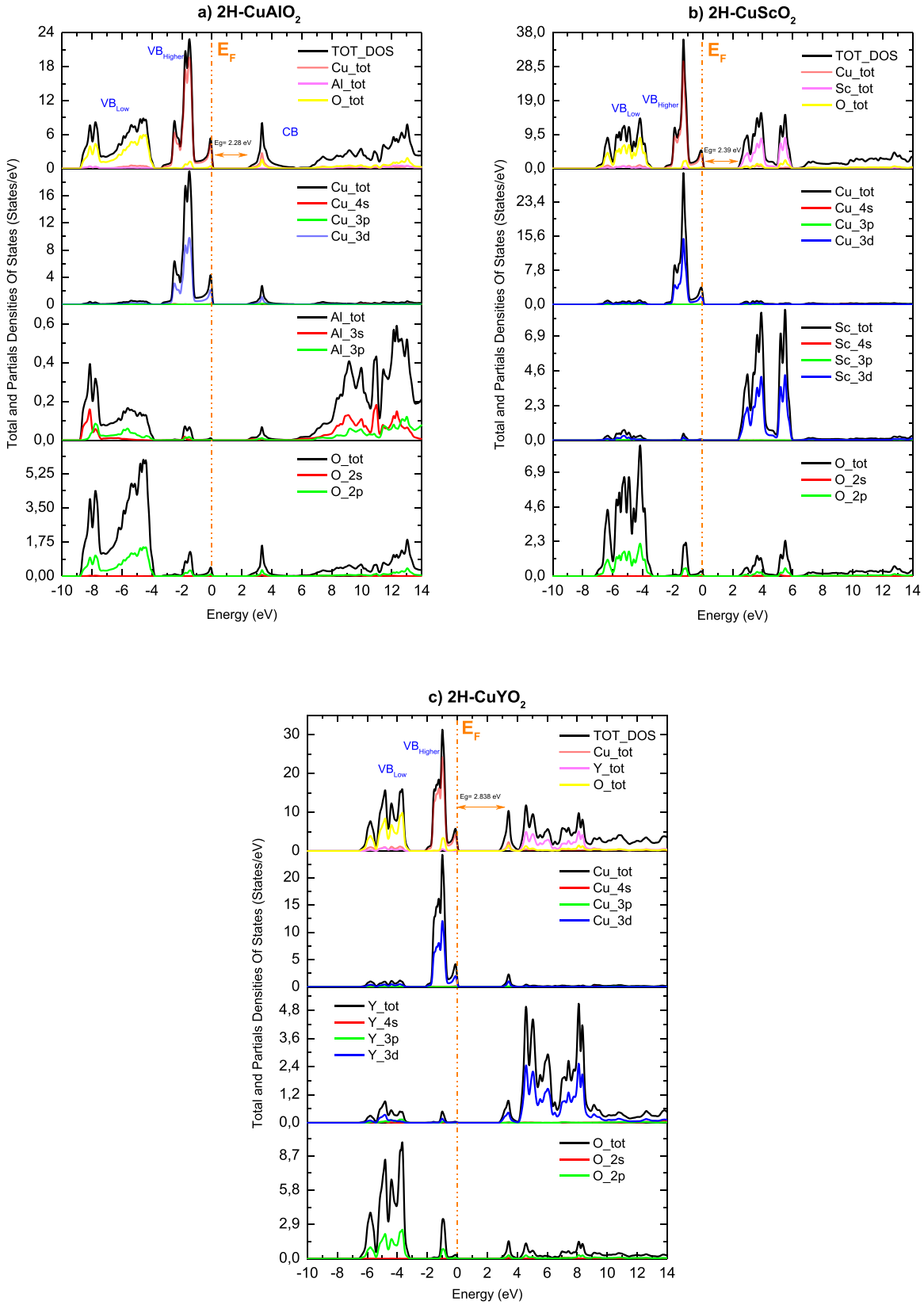

Fig. 6. Partial and total density of states (PDOS and TDOS) for a) $CuAlO_2$, b) $CuScO_2$ and c) $CuYO_2$ within mBJ approximation.

function, refractive index, absorption coefficient, reflectivity, optical conductivity and the electron energy loss have been calculated via TB-mBJ approximation since; the band-gap values are optimized. A dense k-mesh with 2500 k-points (156, 144 and 132 special k-points in the reduced wedge) for $CuAlO_2$, $CuScO_2$ and $CuYO_2$, respectively was used. The linear optical properties were calculated with broadening of 0.1 eV [58].

The complex dielectric function shows how the optical properties of

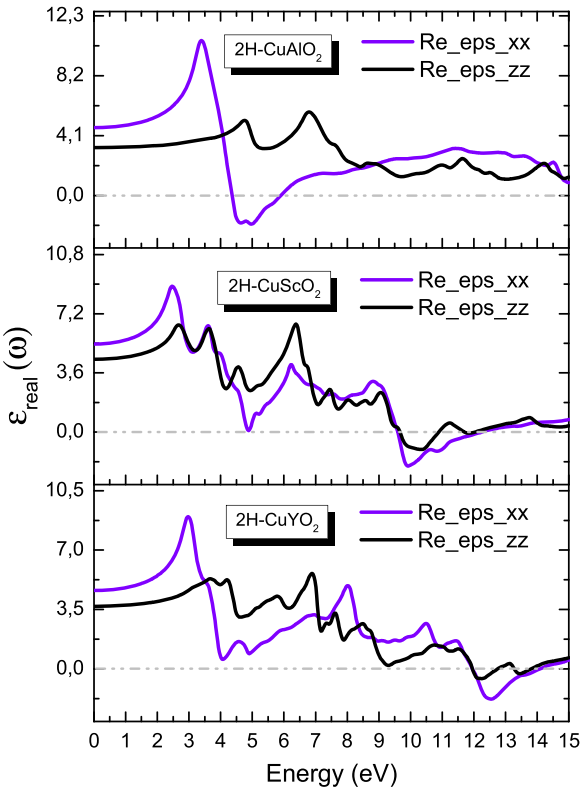

Fig. 7. Calculated real part of the dielectric function for a) $CuAlO_2$, b) $CuScO_2$ and c) $CuYO_2$ within mBJ approximation.

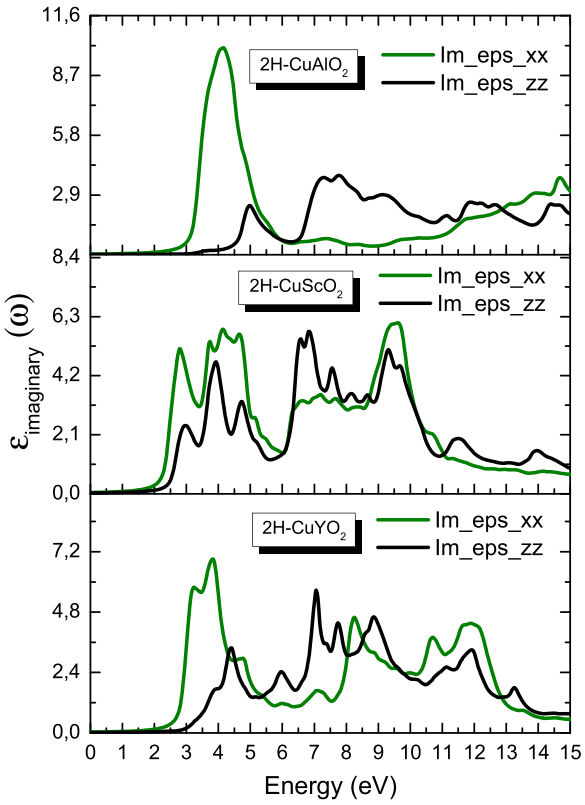

Fig. 8. Calculated imaginary part of the dielectric function for a) $CuAlO_2$, b) $CuScO_2$ and c) $CuYO_2$ within mBJ approximation.

semiconducting materials are dependent on the wavelength of incident light [60] and can be given by $\varepsilon(\omega) = \varepsilon_{real}(\omega) + i\varepsilon_{imaginary}(\omega)$ [61–66]. The real dielectric function would help in calculating other linear optical parameters like refractive index $n(\omega)$, absorption coefficient $\alpha(\omega)$, reflectivity $R(\omega)$, optical conductivity $\kappa(\omega)$ and the electron energy loss $L(\omega)$.

The joint density of state and the momentum matrix elements can help to access inter-band transitions between the VB and CB which are very much important to calculate the $\varepsilon_{imaginary}(\omega)$ [66]. The $\varepsilon_{imaginary}(\omega)$ is given by the following relation [61]:

$$\varepsilon_{imaginary}(\omega) = \frac{e^{2h}}{\pi m^2 \omega^2} \sum \int \left[|M_{c,v}(k)|^2 \delta[\omega_{c,v}(k) - \omega] \right] d^3k \quad (3)$$

The above integral is calculated over BZ, where $M_{c,v}(k)$ represents the dipole moment for direct transitions between VB and CB. $\omega_{c,v}(k) = E_{ck} - E_{vk}$ represents the transition energy and Kramer–Kroning equation would help to deduce the real part $\varepsilon_{real}(\omega)$ of the dielectric function [61, 62]:

$$\varepsilon_{real}(\omega) = 1 + \frac{2}{\pi} p \int_0^{\infty} \frac{\varepsilon_{imaginary}(\omega')}{\omega'^2 - \omega^2} d\omega' \quad (4)$$

From the real and imaginary parts of dielectric function, we can easily deduce the expressions for linear optical properties such as $\alpha(\omega)$, $R(\omega)$, $n(\omega)$, $\kappa(\omega)$ and $L(\omega)$ by the relations given below [61,62,64,66–68]:

$$\alpha(\omega) = \sqrt{2}\omega \left[\sqrt{\varepsilon_{real}^2(\omega) + \varepsilon_{imaginary}^2(\omega)} - \varepsilon_{real}(\omega) \right] \quad (5)$$

$$R(\omega) = \left[\sqrt{\left[\varepsilon_{real}^2(\omega) + i\varepsilon_{imaginary}(\omega) - 1\right]} 2 / \sqrt{\left[\varepsilon_{real}^2(\omega) + j\varepsilon_{imaginary}(\omega) + 1\right]} \right]^2 \quad (6)$$

$$n(\omega) = \frac{1}{\sqrt{2}} \sqrt{\left[\left[\varepsilon_{real}^2(\omega) + \varepsilon_{imaginary}^2(\omega)\right]^{\frac{1}{2}} + \varepsilon_{real}(\omega) \right]} \quad (7)$$

$$\kappa(\omega) = (-i\omega/4\pi)\varepsilon(\omega) \quad (8)$$

$$L(\omega) = Im\left(-\frac{1}{\varepsilon(\omega)}\right) = \frac{\varepsilon_{imaginary}(\omega)}{\varepsilon_{real}^2(\omega) + \varepsilon_{imaginary}^2(\omega)} \quad (9)$$

The linear optical properties of delafossite oxides were predicted by

Table 3
Calculated optical dielectric constant, static reflectivity, static refractive index and $\kappa(\omega)$ peaks for the p-type delafossite transparent conducting oxides 2 H-$CuMO_2$ (M=Al, Sc and Y), within mBJ approximation compared with other previous works.

		2H-$CuAlO_2$		2H-$CuScO_2$		2H-$CuYO_2$	
Optical parameters		*xx*	*zz*	*xx*	*zz*	*xx*	*zz*
$\varepsilon_{imaginary}(0)$	Present work (mBJ)	**4.65**	**3.28**	**5.358**	**4.432**	**4.617**	**3.691**
	Others works	5.07 [24]	3.8 [24]	–	–	–	–
***R*(0)**	Present work (mBJ)	**0.134**	**0.083**	**0.157**	**0.126**	**0.132**	**0.099**
	Others works	–	–	–	–	–	–
***n*(0)**	Present work (mBJ)	**2.16**	**1.81**	**2.31**	**2.1**	**2.15**	**1.92**
	Others works	2.25 [24]	1.9 [24]	–	–	–	–
κ(ω) peak's	Present work (mBJ)	14.68	14.408	9.619	9.319	11.932	8.857

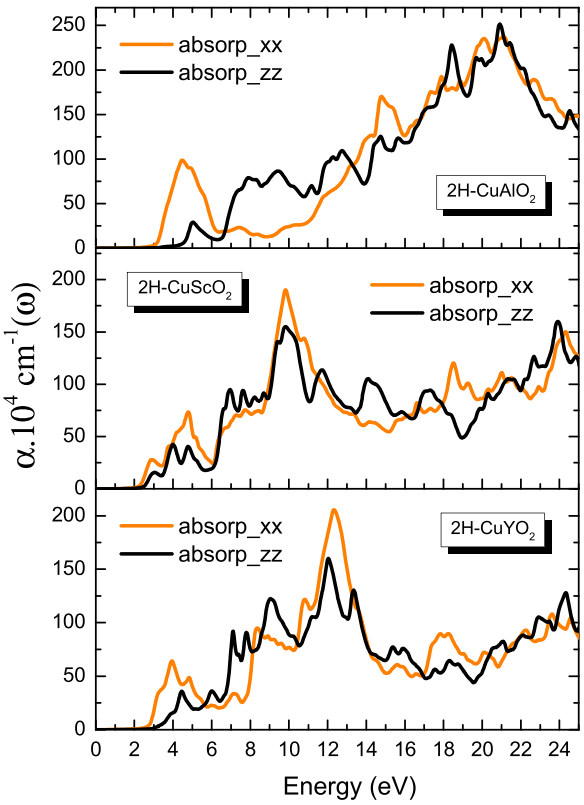

Fig. 9. Calculated absorption coefficient for a) $CuAlO_2$, b) $CuScO_2$ and c) $CuYO_2$ within mBJ approximation.

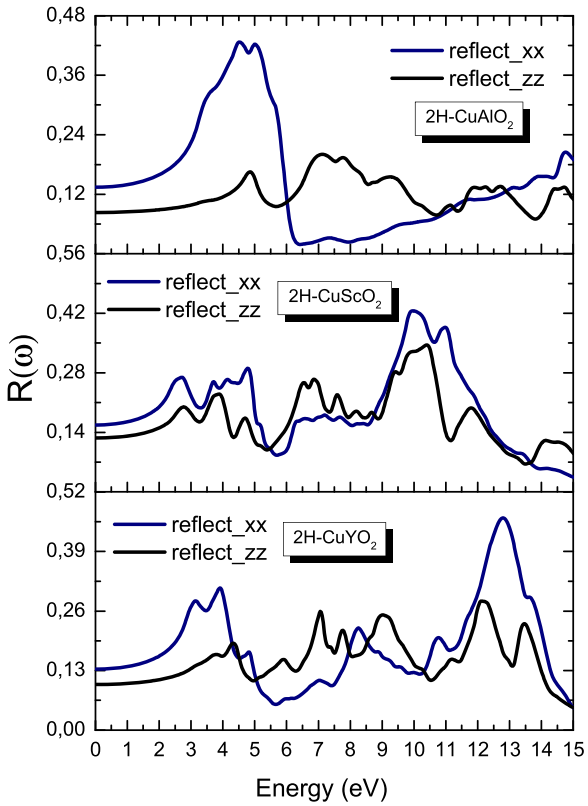

Fig. 10. Calculated reflectivity for a) $CuAlO_2$, b) $CuScO_2$ and c) $CuYO_2$ within mBJ approximation.

considering both types of polarization *i.e.*, ordinary polarization (E⊥c) along *x*, *y* direction and extraordinary polarization (E//c) along *z* direction.

Fig. 7(a-c) display the curves for real part of the dielectric function versus photon energy ranging from 0 to 15 eV. The zero frequency limit ε_{real} (0) is an essential parameter governed by the energy band-gap of the materials [62]. Moreover, the obtained values of static dielectric constant ε_{real} (0) for the three delafossites oxides are listed in Table 3. The $\varepsilon_{real}(\omega)$ has a positive value up to 4.363, 9.590 and 11.952 eV under ordinary polarization and 18.395, 9.661 and 11.954 eV under extraordinary polarization for 2H-$CuAlO_2$, 2H-$CuScO_2$ and 2H-$CuYO_2$, respectively and afterwards, $\varepsilon_{real}(\omega)$ becomes negative. The prominent peaks for real part of dielectric function occur at 3.387, 2.462 and 2.979 eV for 2H-$CuAlO_2$, 2H-$CuScO_2$ and 2H-$CuYO_2$, respectively. The electronic transition from VB to the states of CB resulted in appearance of such peaks.

At higher photon energies, the transparent nature of considered oxides makes these compounds less appropriate for single junction solar cell; although, these materials are suitable for multi-junction or tandem solar cells [30].

The imaginary part of dielectric function i.e., $\varepsilon_{imaginary}$ (ω) represents various real transitions between the occupied and unoccupied states. The characteristics of $\varepsilon_{imaginary}$ (ω) as depicted in Fig. 8(a-c), along the perpendicular and parallel directions to c-axis of light demonstrated the existence of peaks for the incident photon energy up to 15 eV. For 2H-$CuAlO_2$, the peak for $\varepsilon_{imaginary}(\omega)$ appears at 4.149 eV due to its indirect band gap nature. Similarly, for 2H-$CuScO_2$, two peaks appeared, one at 4.149 eV as an evidence of indirect transition in addition to the two more peaks at 6.843 and 9.619 eV. For 2H-$CuYO_2$, three important peaks appeared, the first one at 3.823 eV in addition to the two more peaks at 7.061 and 8.857 eV. Generally, all these peaks are originated from the hybridization bonding and anti-bonding between Cu_3*d*, O_2*p*, Sc_3*d* and Y_3*d* states.

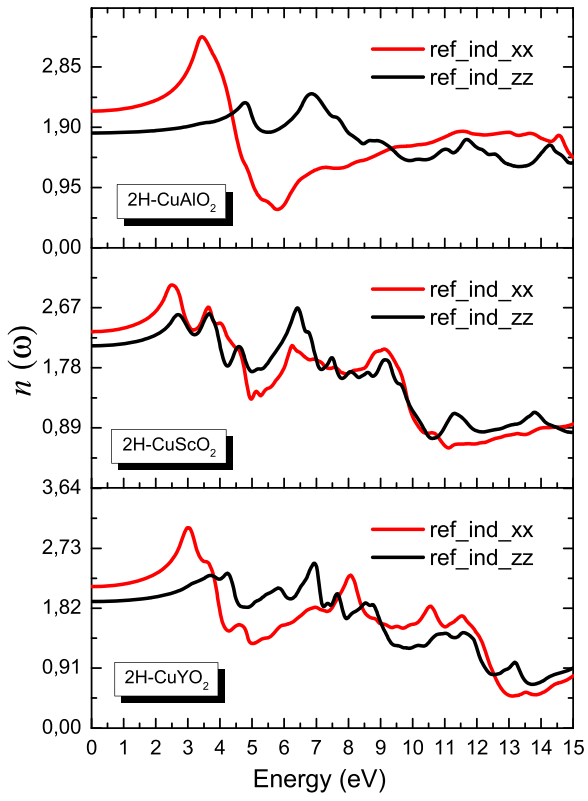

Fig. 11. Calculated refractive index for a) $CuAlO_2$, b) $CuScO_2$ and c) $CuYO_2$ within mBJ approximation.

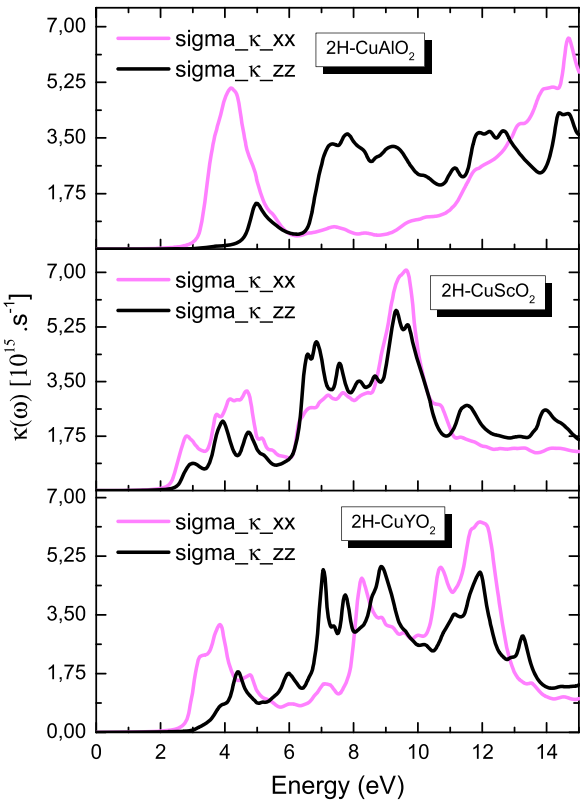

Fig. 12. Calculated conductivity for a) $CuAlO_2$, b) $CuScO_2$ and c) $CuYO_2$ within mBJ approximation.

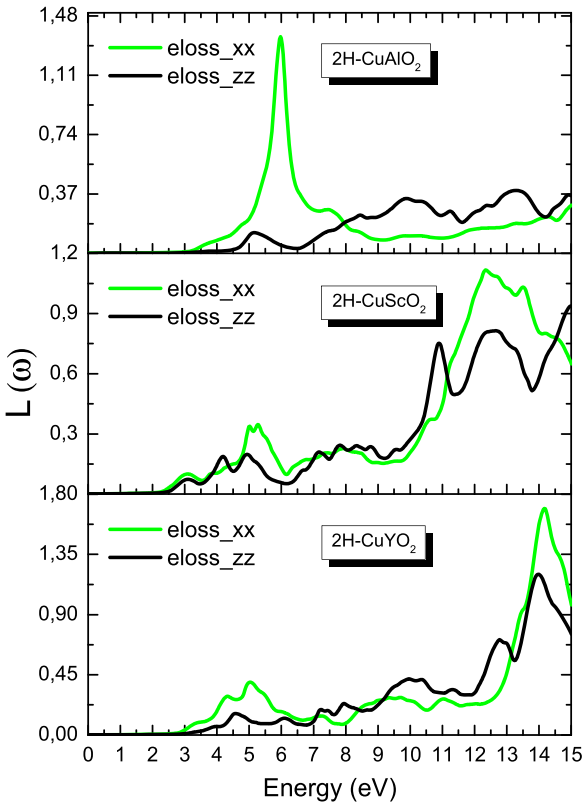

Fig. 13. Energy loss function for a) $CuAlO_2$, b) $CuScO_2$ and c) $CuYO_2$ within mBJ approximation.

The absorption coefficient is one of the important optical parameters and shows a fraction of light that can be observed when passes through the material. The calculated absorption coefficient of longitudinal and parallel components of light for 2H-$CuAlO_2$, 2H-$CuScO_2$ and 2H-$CuYO_2$ within mBJ approximation is illustrated in Fig. 9 for the energy range of incident photon from 0 to 25 eV. A harmonious trend is evident owing to the anisotropic behaviour in context of the polarization type. The absorption edge starts at 2.15, 1.98 and 2.1 eV for the α^{xx} component, and 3.29, 2.24 and 2.92 eV for α^{zz} component for 2H-$CuAlO_2$, 2H-$CuScO_2$ and 2 H-$CuYO_2$, respectively. Furthermore, the first intense peak arises at 20.91 eV for 2H-$CuAlO_2$, at 9.81 eV for 2H-$CuScO_2$ and at 12.34 eV for 2H-$CuYO_2$. The delafossite oxides have demonstrated an improved absorption coefficient that enable the use of maximum energy from the solar spectrum. The observations revealed that these conducting delafossite oxides are suitable when the absorption of light in the visible region of solar spectrum is required. The $CuMO_2$ (M= Al, Sc and Y) materials would have promising applications in solar cells.

The reflectivity of light i.e., R(ω) is a significant linear optical parameter when investigating the p-type delafossite transparent conducting oxides for solar cells. Fig. 10 depicting the low values of R(ω) validates the argument regarding use of these materials in optoelectronic applications. The maximum value for reflectivity is observed at 4.53, 9.94 and 12.8 eV for 2H-$CuAlO_2$, 2H-$CuScO_2$ and 2H-$CuYO_2$, respectively.

The zero frequency reflectivity i.e., R(0) for longitudinal and parallel components of light were obtained using TB-mBJ scheme for photon energy up to 15 eV and are summarized in Table 3.

The refractive index i.e., n(ω) is also one of the important linear optical parameters associated to the atomic interactions microscopic level [69]. The refractive index basically explains the transparency of semiconducting materials as a function of spectral radiations and exhibit an essential role to predict the electronic and optical properties. Moreover, refractive index is a key parameter that has impact on applications like wave-guides, photonic crystals, detectors and solar cells [70]. The calculated n(ω) for delafossite oxides, as a function of the photon energy up to 15 eV is shown in Fig. 11. The most prominent feature of the refractive index in the current study is high intensity peaks in the visible region. These values are obtained within TB-mBJ approximation and are listed in Table 3. The refractive index at lower frequencies can be described as; $n(0) = \sqrt{\varepsilon_{imaginary}}\ (0)$.

The optical conductivity κ(ω) was deduced from the dielectric function as given in Eq. (6). The Fig. 12 depicts the optical conductivity curves of the κ(ω) for photon energy up to 15 eV calculated within TB-mBJ approximation. Numerous optical conductivity peaks are observed for each compound that are observed to vary in accordance with the bulk Plasmon excitations between VB and CB. The locations for highest peaks of the κ(ω) of 2H-$CuAlO_2$, 2H-$CuScO_2$ and 2H-$CuYO_2$ compounds are presented in Table 3.

The L(ω) i.e., electron energy-loss function, defines the loss of electron's energy while making inter band transitions in the valence orbitals. This function includes all the electrons i.e., non-scattered and elastically scattered as given in Eq. (9) [41,71].

Fig. 13 clarified the energy loss function of the three-delafossite oxides within TB-mBJ approximation. The main critical points are situated at 5.972, 12.34 and 14.163 eV for 2H-$CuAlO_2$, 2H-$CuScO_2$ and 2H-$CuYO_2$, respectively. These points represent the lossless regions.

4. Conclusions

In summary, the structural, electronic and optical characteristics of p-type delafossite transparent conducting oxides 2H-$CuMO_2$ (M=Al, Sc and Y) have been investigated. The framework of all-electron FP-LAPW method with LDA and GGA approximations for enhancing the lattice constants, the related bulk modulus B and its first pressure derivative B' have been used. The observations revealed a close agreement among already published experimental and theoretical works. The precise

prediction of energy band-gap, a recently modified semi-local Becke–Johnson potential TB-mBJ has been employed. The band gap calculations revealed that the values obtained are very much reliable when compared with experimental and theoretical calculations. The band structure calculations demonstrated that 2H-CMO_2 is an indirect band gap semiconductor, and for this structure, we have analysed the band-gap structure and other linear optical properties using the TB-mBJ potential. The observed linear optical characteristics of the studied material suggested that the considered materials would have potential applications in solar cells and other optoelectronic devices.

Declaration of Competing Interest

The authors declare that they have no known competing financial interests or personal relationships that could have appeared to influence the work reported in this paper.

Data Availability

No data was used for the research described in the article.

Acknowledgments

M. Hadjab gratefully acknowledges to Professor N. Bouarissa and Professor M. Ibrir from Mohamed Boudiaf University of M'sila (Algeria) for their invaluable helpful discussion. O. Guskova is funded by the German Research Foundation (DFG), project number GU1510/5-1.

References

[1] S. Calnan, A. Tiwari, Thin Solid Films 518 (7) (2010) 1839–1849.
[2] S. Guo, W. Diyatmika, Y. Unutulmazsoy, L. Yang, B. Dai, L. Xu, J. Han, V. Ralchenko, A. Anders, J. Zhu, Appl. Surf. Sci. 585 (2022), 152604.
[3] D.M. Hoat, Phys. B Condens. Matter 558 (2019) 109–115.
[4] L.F.J. Piper, L. Colakerol, A. De Masi, P.-A. Glans, T. Learmonth, K.E. Smith, Phys. Rev. B 79 (2009), 075102.
[5] M.A. Ali, A. Khan, S.H. Khan, T. Ouahrani, G. Murtaza, R. Khenata, S. Bin Omran, Mater. Sci. Semicond. Process. 38 (2015) 57–66.
[6] D. Ginley, Adv. Micro Nanomater. Photovolt. Micro Nano Technol. (2019) 175–194.
[7] A.N. Banerjee, K.K. Chattopadhyay, Prog. Cryst. Growth Charact. Mater. 50 (2005) 52–105.
[8] N. Ray, V. Gupta, L. Sarma, P. Kush, J. Nag, S. Sapra, ACS Omega 3 (2018) 509–513.
[9] Y.H. Kook, D.J. Byun, B.J. Jeon, J.K. Lee, Stud. Surf. Sci. Catal. 159 (2006) 385–388.
[10] S.R. Kodigala, Thin Films Nanostruct. 35 (2010) 505–679.
[11] Z.B. Wang, M.G. Helander, Z.H. Lu, Devices Appl. (2013) 49–76.
[12] T. Minami, MRS Bull. 25 (2000) 38–44.
[13] A. El Maazouzi, R. Masrour, A. Jabar, Phys. B Condens. Matter 631 (2022), 413712.
[14] G. Kadim, R. Masrour, A. Jabar, J. Cryst. Growth 581 (2022), 126509.
[15] N. Baaalla, Y. Ammari, E.K. Hlil, S. Abid, R. Masrour, A. Benyoussef, A. El Kenz, Ceram. Int. 47 (2021) 2338–2346.
[16] G. Kadim, R. Masrour, A. Jabar, E.K. Hlil, Phys. A 573 (2021), 125936.
[17] S. Belhamra, R. Masrour, A. Jabar, E.K. Hlil, Polyhedron 193 (2021), 114891.
[18] G. Kadim, R. Masrour, A. Jabar, Mater. Today Commun. 26 (2021), 102071.
[19] I. Islam, S.A. Khandy, M.B. Zaman, A.K. Hafiz, A.M. Siddiqui, J.-D. Chai, J. Alloy. Compd. 867 (2021), 158900.
[20] H. Hosono, M. Hirano, Nanomater. Res. Appl. (2006) 3–61.
[21] H. Kawazoe, M. Yasukawa, H. Hyodo, M. Kurita, H. Yanagi, H. Hosono, Nature 389 (1997) 939.
[22] P. Lunca-Popa, J. Afonso, P. Grysan, J. Crêpellière, R. Leturcq, D. Lenoble, Sci. Rep. 8 (1) (2018) 7216.
[23] A. Nakanishi, H. Katayama-Yoshida, J. Phys. Soc. Jpn. 85 (2016), 094711.
[24] K.C. Bhamu, R. Khenata, S.A. Khan, M. Singh, K.R. Priolkar, J. Electron. Mater. 45 (1) (2016) 615–623.
[25] A. Buljan, P. Alemany, E. Ruiz, J. Phys. Chem. B 103 (1999) 8060–8066.
[26] P. Poopanya, Phys. Lett. A 379 (9) (2015) 853–856.
[27] R. Liu, Y. Li, B. Yao, Z. Ding, Y. Jiang, L. Meng, R. Deng, L. Zhang, Z. Zhang, H. Zhao, L. Liu, ACS Appl. Mater. Interfaces 9 (14) (2017) 12608–12616.
[28] E. Schiavo, C. Latouche, V. Barone, O. Crescenzi, A.B. Muñoz-García, M. Pavone, Phys. Chem. Chem. Phys. 20 (20) (2018) 14082–14089.
[29] L.-J. Shi, Z.-J. Fang, J. Li, J. Appl. Phys. 104 (2008), 073527.
[30] N.N. Som, V. Sharma, V. Mankad, M.L.C. Attygalle, P.K. Jha, Sol. Energy 193 (2019) 799–805.
[31] H.A.R. Aliabad, Z. Sabazadeh, A. Abareshi, Rare Met. 38 (2019) 905–913.
[32] W. Lan, W.L. Cao, M. Zhang, X.Q. Liu, Y.Y. Wang, E.Q. Xie, H. Yan, J. Mater. Sci. 44 (2009) 1594–1599.
[33] N. Benreguia, A. Barnabé, M. Trari, J. Sol. Gel Sci. Technol. 75 (2015) 670–679.
[34] Y. Liu, Y. Gong, N.P. Mellott, B. Wang, H. Ye, Y. Wu, Sci. Technol. Adv. Mater. 17 (1) (2016) 200–209.
[35] C.H. Shih, B.H. Tseng, Phys. Procedia 32 (2012) 395–400.
[36] W.C. Sheets, E. Mugnier, A. Barnabé, T.J. Marks, K.R. Poeppelmeier, Chem. Mater. 18 (1) (2006) 7–20.
[37] P. Blaha, K. Schwarz, G.K.H. Madsen, D. Kvasnicka, J. Luitz, WIEN2k, An Augmented Plane Wave Plus Local Orbital Program for Calculating Crystal Properties, Vienna University of Technology, Vienna, Austria, 2001.
[38] P. Hohenberg, W. Kohn, Phys. Rev. B 136 (1964) 864–871.
[39] W. Kohn, L.S. Sham, A1133, Phys. Rev. 140 (1965) 1133–1138.
[40] S. Blügel, G. Bihlmayer, Comput. Nanosci. NIC Ser. 31 (2006) 85–129.
[41] M. Hadjab, S. Berrah, H. Abid, M.I. Ziane, H. Bennacer, A.H. Reshak, Mater. Chem. Phys. 182 (2016) 182–189.
[42] J.P. Perdew, Y. Wang, Phys. Rev. B 45 (1992) 13244.
[43] J.P. Perdew, A. Zunger, Phys. Rev. B 23 (1981) 5048.
[44] J.P. Perdew, A. Ruzsinszky, G.I. Csonka, O.A. Vydrov, G.E. Scuseria, L. A. Constantin, X. Zhou, K. Burke, Phys. Rev. Lett. 100 (2008), 136406.
[45] F. Tran, P. Blaha, Phys. Rev. Lett. 102 (2009), 226401.
[46] A.D. Becke, M.R. Roussel, Phys. Rev. A 39 (1989) 3761.
[47] F.D. Murnaghan, Proc. Natl. Acad. Sci. USA 30 (1944) 244–247.
[48] B.U. Köhler, M. Jansen, Z. Anorg. Allg. Chem. 543 (1986) 73–80.
[49] K. Isawa, Y. Yaegashi, M. Komatsu, N. Nagano, S. Sudo, M. Karppinen, H. Yamauchi, Phys. Rev. B 56 (1997) 3457.
[50] M.N. Huda, Y. Yan, A. Walsh, S.-H. Wei, M.M. Al-Jassim, Phys. Rev. B 80 (2009), 035205.
[51] H.C. Kandpal, R. Seshadri, Solid State Sci. 4 (2002) 1045.
[52] B.U. Köhler, M. Jansen, Z. Krist. Cryst. Mater. 165 (1983) 313.
[53] T. Ishiguro, N. Ishizawa, N. Mizutani, M. Kato, J. Solid State Chem. 49 (1983) 232.
[54] S.A. Khandy, Sci. Rep. 11 (2021) 20756.
[55] W.T. Liu, Y.Y. Luo, Z.T. Liu, Z.M. We, Appl. Mech. Mater. 252 (2013) 263–266.
[56] R. Gillen, J. Robertson, Phys. Rev. B 84 (2011), 035125.
[57] H. Yanagi, S. Inoue, K. Ueda, H. Kawazoe, H. Hosono, N. Hamada, J. Appl. Phys. 88 (2000) 4159.
[58] A. Delin, Opt. Commun. 167 (1999) 105–109.
[59] S.A. Khandy, S.G. Vaid, I. Islam, A.K. Hafiz, J.-D. Chai, J. Alloy. Compd. 867 (2021), 158966.
[60] K.M. Kosuda, J.M. Bingham, K.L. Wustholz, R.P. Van Duyne, R.J. Groarke, Comprehensive Nanoscience and Nanotechnology (Second Edition), 4 (2016) 117 – 152.
[61] M. Hadjab, S. Berrah, H. Abid, M.I. Ziane, H. Bennacer, B.G. Yalcin, Optik 127 (2016) 9280–9294.
[62] M. Hadjab, M. Ibrir, S. Berrah, H. Abid, M.A. Saeed, Optik 169 (2018) 69–76.
[63] A. Hadj Larbi, S. Hiadsi, M. Hadjab, M.A. Saeed, Optik 166 (2018) 169–176.
[64] M.I. Ziane, M. Tablaoui, A. Khelfane, M. Hadjab, H. Bennacer, Optik 157 (2018) 248–258.
[65] M.I. Ziane, H. Bennacer, M. Mostefaoui, M. Tablaoui, M. Hadjab, A. Saim, K. Bekhedda, Optik 243 (2021), 167490.
[66] H. Bennacer, A. Boukortt, S. Meskine, M. Hadjab, M.I. Ziane, A. Zaoui, Optik 159 (2018) 229–244.
[67] X. Ma, D. Li, S. Zhao, G. Li, K. Yang, Nanoscale Res. Lett. 9 (580) (2014) 1–8.
[68] Q.-J. Liu, Z.-T. Liu, J.-C. Chen, L.-P. Feng, H. Tian, Phys. B 406 (2011) 3377–3382.
[69] H. Bennacer, S. Berrah, A. Boukortt, M.I. Ziane, Indian J. Pure Appl. Phys. 53 (2015) 181–189.
[70] N.M. Ravindra, P. Ganapathy, J. Choi, Infrared Phys. Technol. 50 (2007) 21–29.
[71] K. Bougherara, F. Litimein, R. Khenata, E. Uçgun, H.Y. Ocak, Ş. Uğur, G. Uğur, A. H. Reshak, F. Soyalp, S. Bin-Omran, Sci. Adv. Mater. 5 (2013) 1–10.